Pharm Res (2015) 32:2663–2677
DOI 10.1007/s11095-015-1651-0

RESEARCH PAPER

Overexpressed Macrophage Mannose Receptor Targeted Nanocapsules- Mediated Cargo Delivery Approach for Eradication of Resident Parasite: *In Vitro* and *In Vivo* Studies

Shalini Asthana • Pramod K. Gupta • Anil K. Jaiswal • Anuradha Dube • Manish K. Chourasia

Received: 5 November 2014 / Accepted: 4 February 2015 / Published online: 27 February 2015

ABSTRACT

Purpose Since, *Leishmania* protozoans are obligate intracellular parasites of macrophages, an immunopotentiating macrophage-specific Amphotericin B (AB) delivery system would be ideally appropriate to increase its superiority for leishmaniasis treatment and to eliminate undesirable toxicity. Herein, we report AB entrapped mannose grafted chitosan nanocapsules (*Mnos*CNc-AB) that results in effective treatment of visceral leishmaniasis, while also enhancing *L. donovani* specific T-cell immune responses in infected host.

Methods *Mnos*CNc-AB were prepared via synthesized mannosylated chitosan deposition on interface of oil/water nanoemulsion intermediate and were characterized. J774A.1 macrophage uptake potential, antileishmanial activity and immunomodulatory profile were evaluated in hamster. Tissue localization, biodistribution and toxicity profile were also investigated.

Results *Mnos*CNc-AB had nanometric size (197.8 ± 8.84 nm), unimodal distribution (0.115 ± 0.04), positive zeta potential (+31.7 ± 1.03 mV) and 97.5 ± 1.13% cargo encapsulation efficiency. Superior macrophage internalization of mannosylated chitosan nanocapsules compared to unmodified chitosan nanocapsules was observed by fluorescence-based assessment, further confirmed by rapid blood clearance and, greater localization and higher accumulation in macrophage rich liver and spleen. While, *Mnos*CNc-AB mediated cargo distribution to kidney decreased. Augmented *in vitro* antileishmanial activity and *in vivo* pro-inflammatory mediator's expression were observed with *Mnos*CNc-AB, led to significant reduction (~90%) in splenic parasite burden.

Conclusions Results demonstrated that mannose ligand grafted chitosan nanocapsules could improve selective delivery of AB into macrophages via interactions with overexpressed mannose receptors thus reduce undesirable toxicity. Study provides evidence for *Mnos*CNc-AB potential to leishmaniasis therapeutics and presents valuable therapeutic strategies for combating chronic macrophage-resident microbial infections.

KEY WORDS cytokines · visceral leishmaniasis

ABBREVIATIONS

AB	Amphotericin B
ALAT	Alanine aminotransferase
BSA	Bovine serum albumin
BUN	Blood urea nitrogen
CNc	Chitosan nanocapsules
CRDs	Carbohydrate recognition domains
CS	Chitosan
DL	Drug loading
DMSO	Dimethyl sulfoxide
EE	Encapsulation efficiency
FAB	FITC tagged AB
FITC	Fluorescein isothiocyanate
HPRT	Hypoxanthine phosphoribosyltransferase
IFN-γ	Interferon gamma
IL-10	Interleukin 10
IL-12	Interleukin 12
IL-4	Interleukin 4
iNOS	Inducible NO synthase
MMRs	Macrophage mannose receptors

Electronic supplementary material The online version of this article (doi:10.1007/s11095-015-1651-0) contains supplementary material, which is available to authorized users.

S. Asthana • P. K. Gupta • M. K. Chourasia (✉)
Pharmaceutics Division, Council of Scientific and Industrial Research-Central Drug Research Institute, B 10/1, Sector 10, Jankipuram Extension, Sitapur Road, Lucknow, UP 226 031, India
e-mail: manish_chourasia@cdri.res.in

A. K. Jaiswal • A. Dube
Parasitology Division, Council of Scientific and Industrial Research-Central Drug Research Institute, B 10/1, Sector 10, Jankipuram Extension, Sitapur Road, Lucknow 226031, India

*Mnos*CNc	Mannosylated chitosan nanocapsules
Mnos-CS	Mannosylated chitosan copolymer
MPS	Mononuclear phagocyte system
MRT	Mean residence time
MTT	-[4, 5-dimethylthiazol-2-yl]-2, 5-diphenyltetrazolium bromide
NO	Nitric oxide
PAMPs	Pathogen-associated molecular patterns
PDI	Polydispersity index
PI	Parasite inhibition
TGF-β	Transforming growth factor beta
TNF-α	Tumor necrosis factor alpha

INTRODUCTION

Although there has been noteworthy progress in the development of new chemotherapeutic strategies, intra-macrophage diseases still present challenges. Currently used chemotherapeutic cargos are systemically efficient but not selective for macrophage resident intracellular parasites. Thus results in severe undesirable side effects such as nephrotoxicity, hepatotoxicity and hematotoxicity (1,2), which limit the cargo dose that can be allowable for administration. Consequently, significant efforts are necessary to develop alternative strategies that improve the therapeutic window of chemotherapeutic cargos both by increasing efficiency and decreasing related toxicity.

Promising ligand directive actively targeted nanoparticulate mediated cargo delivery approach has great therapeutic potential for a variety of intra-macrophage diseases i.e., leishmaniasis, tuberculosis, filariasis and Chagas' disease. Nanoparticulate systems can be delivered to particular sites through size-/potential-based passive targeting or through active targeting by attachment of biomarker specific ligands (3). Delivery system conjugated with targeting ligand (i.e., antibodies, sugar, vitamins) could achieve an elevated degree of selectivity to specific organ and augment the internalization of encapsulated cargo into particular cells.

Notably, after parasite infection molecular machineries of macrophages get modulated and results in overexpression of varieties of glycoproteins such as macrophage mannose receptors (MMRs; CD206), lectin receptors, scavenger receptors and stearylamine receptors (3–5), that have ability to bind with "identifiable" pathogen-associated molecular patterns (PAMPs) and can be utilized as biomarkers for particular pathogenic condition. Specifically, MMR is 175-kD cell-surface transmembrane glycoprotein composed of a N-terminal cysteine-rich domain (Cys-MR), a fibronectin type II domain and eight tandemly arranged C-type lectin-like carbohydrate recognition domains (CRDs) (6). The CRDs of the extracellular region mediate calcium-dependent binding to sugars such as mannose, fucose and N-acetylglucosamine that are PAMPs, commonly found on the cell surfaces of a wide array of infectious agents and transport them into endocytic pathways (7). Consequently, overexpressed MMRs can efficiently be targeted with appropriate mannosylated cargo-delivery systems having mannose moiety as PAMPs, may correlate with improvement of receptor-mediated uptake upon receptor binding.

In previous study we have developed chitosan based delivery system i.e., chitosan (CS) nanocapsules (CNc) as nanocarrier for Amphotericin B (AB)-mediated antileishmanial chemotherapy, showed acceptable low AB mediated unwanted cellular toxicity (8). However, chitosan based delivery systems are reported to have narrow cell (macrophage) specificity which limits its biomedical application for more specific macrophage targeted drug delivery (9). To our knowledge, to date, there has been no report examining the effect of surface modification of AB encapsulated CNc with mannose (*Mnos*CNc-AB) on their antileishmanial potential, macrophage targetibility, biodistribution and toxicity evaluation *in vivo*. On these premises, with the intention to improve chitosan biomedical application, and decrease toxic manifestations of AB, in this study, mannosylated chitosan copolymer (*Mnos*-CS) was synthesized and subsequently, formulated in nanocapsule system (*Mnos*CNc) for AB delivery. Developed AB-nanoreservoir was then investigated for how altering the surface properties of these nanocapsules affected their interaction with macrophages *in vitro*, antileishmanial activity against *L. donovani*-infected macrophages and hamsters, immune-alteration and biodistribution characteristics *in vivo*. Toxicity assay was also performed to determine the biocompatibility of these carrier systems.

MATERIAL AND METHODS

Materials

Mannopyranosylphenyl isothiocyanate, soya lecithin, soyabean oil, Tween 80, low molecular weight chitosan (75–85% deacetylation and 20–200 cps. viscosity), 3-[4, 5-dimethylthiazol-2-yl]-2, 5-diphenyltetrazolium bromide (MTT) and fluorescein isothiocyanate (FITC) were supplied by Sigma-Aldrich (MO, USA). Intas Pharmaceuticals (Ahmadabad, India) kindly provided Amphotericin B. Dialysis membrane (cut-off mol. wt. 12 KD) and potassium dihydrogen phosphate (KH_2PO_4) were purchased from HiMedia (Mumbai, India). For cell culture, all components were from Sigma-Aldrich. HPLC grade acetonitrile and methanol were supplied from SD Fine Chem Ltd (Mumbai, India). All other chemicals were of analytical grade.

Animals and Parasites

Syrian golden hamsters (45–50 g), Wistar rats (150–200 g) and Swiss mice (18–20 g), bred in the institutional animal facility,

were utilized for the studies. The studies were approved by the Institutional Animal Ethics Committee (IAEC) and performed according to the guidelines of the Council for the Purpose of Control and Supervision of Experiments on Animals (CPCSEA), Government of India. The WHO reference strain of *Leishmania donovani* (MHOM/IN/80/Dd8) was used for *in vitro* and *in vivo* experiments. Parasites and the J774A.1 macrophage cell line were maintained in RPMI-1640 medium (Sigma-Aldrich, MO, USA) supplemented with 10% heat inactivated fetal bovine serum (HIFBS) (Sigma-Aldrich, MO, USA), 100 U/ml penicillin and 100 μg/ml streptomycin at 37°C in humidified atmosphere of 5% (*v*/*v*) CO_2/air mixture (8).

Synthesis and Characterization of *Mnos*-CS

Mannose sugar-bound chitosan (*Mnos*-CS) was synthesized by the reaction between amine groups of chitosan and isothiocyanate groups of α-D-mannopyranosylphenyl isothiocyanate, using the method reported previously (10) with minor modifications. Briefly, chitosan solution (70 mg/ml distilled water) was mixed with equal volume of mannopyranosylphenyl isothiocyanate solution (5 mg/ml DMSO) and stirred (IKA, Germany) for 24 h at room temperature. The synthesized white solid mass of *Mnos*-CS was precipitated by adding isopropanol and centrifuged at 12,000 rpm for 15 min. After repeating this process five times, the pellets were freeze-dried.

Functionalization of polymer was confirmed by Fourier transform infrared spectroscopy (FTIR, Perkin-Elmer, Buckinghamshire, United Kingdom) equipped with spectrum v3.02 software. The copolymer, *Mnos*-CS was characterized to identify N-CS bond and thus to ascertain that CS is covalently bound to mannose anchor. For IR spectrum, *Mnos*-CS and CS were incorporated into a KBr disc and run on a FT-IR single beam spectrometer.

Formulation of AB Encapsulated Mannosylated Chitosan Nanocapsules

Nanocapsules were prepared using polymer deposition technique on the interface of oil/water nanoemulsion intermediate (11), where nanoemulsion was obtained by emulsification solvent evaporation method (12). To obtain nanoemulsion intermediate, aqueous phase consisted of 4% (*w*/*w*) Tween 80, 2.25% (*w*/*w*) glycerol and water, was emulsified in oil phase containing 10% (*w*/*w*) soyabean oil, 3% (*w*/*w*) soya lecithin, acidic methanolic AB cargo solution and ethanol, by supplying ultrasonic energy (SONICS, USA) for 4 min at 40% amplitude (20 s pulse on and 5 s pulse off), followed by solvent evaporation. Subsequently, equimolar mixture of 0–1.6%*w*/*v* polymer [either preformed CS or synthesized *Mnos*-CS to obtain chitosan nanocapsules (CNc) or mannosylated chitosan nanocapsules (*Mnos*CNc), respectively] and ethanol was gradually added within the continuous aqueous phase of the nanoemulsion intermediate in 1:10 ratio followed by stirring at room temperature for complete solvent evaporation. The nanocapsules were collected by centrifugation (Beckman Coulter, Fullerton, CA, USA) at 50,000×*g* for 20 min, followed by twice washing with distilled water to remove excess emulsifier before lyophilization. Different cryoprotectants were screened for effective lyophilization of nanocapsule formulations and sucrose (2.5%*w*/*v*) was found to be highly efficient cryoprotectant (Table S1 and S2).

Nanocapsule Characterization

Particle Size, Distribution and Zeta Potential

The mean particle size and size distribution (polydispersity index, PDI) of nanocapsules were analyzed by photon correlation spectroscopy (PCS) at 25°C under an angle of 90°. Zeta potential was determined using laser Doppler anemometry (LDA) at 25°C using a Zetasizer (Nano ZS, Malvern Instrument, Worcestershire, UK) just after dispersion in distilled water.

Encapsulation Efficiency and Cargo Loading

To quantify the encapsulated AB content, a certain amount of the nanocapsules was dispersed in dimethyl sulfoxide, vortexed and centrifuged for 20 min at 2000×*g*. After that, 1 volume of the supernatant was mixed with 9 volume of methanol and resultant solution was quantified for AB content by high performance liquid chromatography (HPLC) (LC-10ATvp, Shimadzu, Tokyo, Japan) method using a Lichrosphere reverse-phase C_{18} column (250×4 mm, 5 μm; Merck, Darmstadt, Germany) using acetonitrile with KH_2PO_4 (pH 3.5), (60:40, *v*/*v*) as mobile phase with 1.0 ml/min flow rate and column effluent was detected with a UV detector at 405 nm.

The AB encapsulation efficiency (%EE) and drug (cargo) loading (%DL) were expressed as the percentage of the drug amount found in the nanocapsules to the total amount used to prepare the nanocapsules and the percentage of the drug amount found in the nanocapsules, respectively.

In Vitro AB Release Study

The *in vitro* encapsulated cargo release from the carriers was evaluated using dialysis membrane diffusion technique under sink conditions. Briefly, 2 mg AB equivalent of formulation or native AB was suspended in 1 ml of phosphate buffer solution (PBS, pH 7.4), filled within dialysis tubing and dialyzed against 250 ml of PBS with 0.5%*v*/*v* Tween 80 using dissolution apparatus (DISSO 2000, Labindia, India), thermostated at 37 ± 1°C with 100 rpm moderate shake. At predetermined

intervals, a definite volume (1 ml) of the release medium was withdrawn and replaced with fresh PBS. Withdrawn samples were filtered through 0.22 μm filter and quantified for the amount of AB released using HPLC method as described in previous section. Each measurement was executed in triplicate and reported as their average.

Stability Study

Test samples at an equivalent concentration of 1 mg AB/ml were incubated with 10% bovine serum albumin (BSA) and 10% plasma (separated from Wistar rat blood) at room temperature. At each time point, an aliquot of the sample was collected to monitor variation in size and encapsulated drug content.

Assessment of Targeting Effect of Nanocapsules

Tagging of AB with FITC Fluorochrome

To examine the *in vitro* macrophage uptake and *ex vivo* tissue localization study, AB cargo was labeled with FITC fluorochrome as described previously (13). Briefly, AB (10 mg) and FITC (5 mg) were dissolved in dimethylacetamide (2 ml) in 5 ml round bottom flask. Subsequently, 200 μL triethylamine was added as base catalyst and reaction mixture was stirred for 2 h at room temperature. Thereafter, ethyl acetate (10 ml) was added to precipitate the reaction product, separated by centrifugation at 18,000×*g* for 10 min and dried over desiccant under vacuum. TLC of the reaction product, AB cargo and FITC was performed using a mobile phase consisted of ethyl acetate: methanol (2:3) to identify formation of FITC tagged AB (FAB).

Macrophage Uptake of Fluorescent Nanocapsules

FAB was encapsulated within nanocapsules in the same manner as described in the formulation section replacing AB with FAB. The J774A.1 cell cultures were incubated in 5% CO_2 environment in RPMI-1640 medium with FITC tagged formulations (CNc-FAB and *Mnos*CNc-FAB) and FAB at 10 μg/ml equivalent concentration for 6 h at 37°C. After trypsinization, cells were transferred in vials and relative cell-associated fluorescence was analyzed by fluorescence activated cell sorter (FACS) instrument (BD Biosciences, FACS Aria, Heidelberg, Germany) at λ_{EX} (485 nm) and λ_{EM} (538 nm).

Ex Vivo Imaging

The Swiss mice were injected with fluorescent FAB encapsulated nanocapsule formulations and FAB at 0.5 mg FAB/kg dose, via the tail vein consecutively for 3 days. Two hour after last administration, the mice were sacrificed and their spleen, liver, lung, kidney and heart were isolated, washed with PBS, fixed, embedded in wax and sectioned using microtome (LEICA RM 2155, Germany) and images were taken using fluorescent microscope (Leica, DMRBE, Bensheim, Germany).

In Vivo Distribution of AB Loaded Nanocapsules

For this study, male Wistar rats were randomly divided into three groups ($n=3$) to receive CNc-AB, *Mnos*CNc-AB, or plain AB (1 mg AB/kg), while maintaining the dose volume to be intravenously injected at 0.2 ml per rat of approximately 200 g weight. Subsequently, blood was collected by cardiac puncture at all the time points starting from 0.5 to 48 h and animals were sacrificed to collect liver, spleen, heart, kidney and lung. Plasma samples obtained from collected blood (0.5 ml) were deproteinized with methanol (1:1). Tissue (0.5 g) samples were homogenized with 2 ml of distilled water over an ice bath and 300 μl homogenate was added to 900 μl methanol, followed by vortex (30 s) and centrifugation. The filtered supernatant of processed plasma and tissues were used for quantification of AB using HPLC method as described previously. The pharmacokinetic parameters were calculated using the WinNonlin 5.0.1 software (version 2.0). The non-compartmental approach was applied for data analysis following i.v. administrations of AB-formulations.

Assessment of Antileishmanial Activity and Immune-Alteration Profile

In Vitro Assessment of Antileishmanial Activity

An *in vitro* macrophage model was used to assess the antileishmanial activity of AB-formulations against intramacrophage amastigotes and study was executed according to protocol followed previously (14). Different cargo dilutions of CNc-AB, *Mnos*CNc-AB, or plain AB, and cargo-free nanocapsules amount equivalent to cargo encapsulated formulations were added in wells triplicate with three untreated control wells to macrophages (1×10^5 cells/well) pre-infected with promastigotes expressing green fluorescent protein (GFP) at multiplicity of 10 *L. donovani* parasites per macrophage. Cells were removed 48 h post-incubation, washed in PBS and parasite associated fluorescence was quantitated by flow cytometry at λ_{EX} (488 nm) and λ_{EM} (515 nm). Multi-parametric data analysis was performed using Kaluza software (Becton Dickinson). The percentage of parasite death was determined by measuring relative fluorescence levels of treated parasites with that of untreated control parasites. Dose response curves were plotted and inhibitory concentrations (IC_{50} and IC_{90}) against intracellular amastigotes were determined.

In Vivo Assessment of Antileishmanial Activity

Twenty five hamsters were infected by intracardiac injection of 1×10^8 *L. donovani* promastigotes. After 30 days, the infection was monitored in five randomly selected hamsters by splenic biopsy and processing of splenic dab. Four treatment hamster groups ($n=5$) were injected intraperitoneally with CNc-AB, *Mnos*CNc-AB, plain AB cargo or PBS (for control group) at 1 mg/kg body weight per day in a constant volume of 200 µl for five consecutive days. One week post-treatment, splenic biopsies were performed on all animals and amastigotes counts were assessed microscopically through Giemsa-stained imprints. The percentage parasite inhibition (PI) was calculated using the formula: $PI=(PP-PT/PP)\times100$ where PP is the number of amastigotes per 100 macrophage nuclei in spleen before treatment whereas PT is the number of amastigotes per 100 macrophage nuclei after treatment.

In Vivo Assessment of Immune-Alteration Profile

The mRNAs expression level of cytokines and inducible NO synthase (iNOS) in splenic culture supernatants from experimental hamsters were determined through quantitative real time-PCR (qRT-PCR, Bio-Rad, USA). Splenic tissues were harvested from experimental hamster groups, total mRNA was extracted using TRI reagent (Sigma-Aldrich, USA) and quantified using Gene-quant (Bio-Rad, USA). One microgram of mRNA was transcribed into cDNA using a first-strand cDNA synthesis kit (Fermentas, USA). qRT-PCR was performed as per the protocol described earlier (15), under conditions: initial denaturation at 95°C for 2 min followed by 40 cycles, each consisting of denaturation at 95°C for 30 s, annealing at 55°C for 40 s, and extension at 72°C for 40 s per cycle. cDNAs from infected untreated hamsters were utilized as comparator samples. PCR signals were quantified by comparing the cycle threshold (CT) value of gene of interest with the cycle threshold value of reference gene hypoxanthine phosphoribosyltransferase (HPRT). Data were expressed as relative fold change (FC) in mRNA of treated groups compared with that of untreated infected hamsters.

Safety Assessment Assay

In Vitro Assessment

Hemo-compatibility Assessment. Hemo-compatibility strength of AB-nanocapsules was evaluated against erythrocytes (16), which were isolated from the whole heparinized blood of Wistar rats by centrifugation (at 1500×*g* for 20 min). The sedimented erythrocytes were washed thrice with PBS and stock was prepared by mixing centrifuged erythrocytes with PBS (pH 7.4) in 3:11 ratio and 100 µl of stock was further utilized to obtain 1 ml functional erythrocyte suspension. AB-formulations equivalent to 0.5–25 µg AB/ml were incubated with erythrocytes at 37°C for 2 h followed by centrifugation at 9300×*g* (20 min) to separate intact erythrocytes and supernatant was sequentially taken into 96 well plates. The hemoglobin released into the supernatant was measured by taking absorbance at 576 nm using a multiwell microplate reader (BIO-TEK, Model-Power wave XS, Crailsheim, Germany). Erythrocytes mixed with distilled water and with PBS were considered as positive and negative control, respectively. Percentage hemolysis was calculated by using the equation:

$$\%\ \text{hemolysis} = (\text{ABs}-\text{ABs}_0)\Big/(\text{ABs}_{100}-\text{ABs}_0)\times100$$

Where ABs, ABs_0 and ABs_{100} are absorbance of test sample, negative control and positive control, respectively. All experiments were performed in triplicate.

Cytotoxicity Assessment on J774A.1 Murine Macrophages Cell Line. Quantitative colorimetric MTT assay was used for measurement of metabolically active J774A.1 cells and used for determining half maximal cytotoxic concentration (CC_{50}) value of *L. donovani* treated with AB-formulations. Briefly, 1×10^6 cells per well in triplicate were treated with increasing concentration of CNc-AB, *Mnos*CNc-AB and plain AB (0.5–25 µg/ml) and three untreated wells for macrophages were considered as control. Following 48 h incubation, the supernatant was replaced with RPMI containing MTT (500 µg/ml) and further incubated for 4 h as described previously by our group (8). To solubilise the resulting formazan crystals, 100 µl of DMSO was added and optical density of well content measured at 570 nm using a multiwell microplate reader. The percentage of cell viability was expressed as the ratio between the amount of formazan determined for treated cells and for control non-treated cells.

In Vivo Assessment

Subacute Toxicity. Mice groups ($n=3$) injected intravenously with CNc-AB, *Mnos*CNc-AB, plain AB cargo or PBS (for control group) each at the dose of 1 mg/kg body weight in a constant volume of 200 µl daily for 14 days. Twelve hours post-treatment, blood was collected from animals by cardiac puncture, centrifuged and colorimetrically analyzed for various biochemical parameters, i.e., transaminase activities, blood urea nitrogen (BUN) and creatinine using an automatic Hitachi 912 apparatus (Roche Diagnostics Corporation, Indianapolis, IN, USA).

Single Dose Acute Toxicity Studies. Mice groups ($n=6$) were administered with various doses of AB either as CNc-AB (5, 10 and 20 mg/kg), *Mnos*CNc-AB (5, 10 and 20 mg/kg) or as plain cargo (1, 2 and 5 mg/kg) through intraperitoneal route

after required dilution with 5% sterile dextrose solution. Survival was followed up to 8 h and animal mortality was examined.

$$\%\ \text{Mortality rate} = \left(\text{Number of dead mice} \Big/ \text{Total number of mice}\right) \times 100$$

Statistical Analysis. Results were expressed as mean ± SD. All data were generated in three independent experiments. Statistical analysis was performed with one-way analysis of variance (ANOVA). Differences were considered to be statistical significant at a level of $P < 0.05$.

RESULTS

Characterization of Mannosylated Chitosan (Mnos-CS) Copolymer

The synthetic scheme of *Mnos*-CS copolymer has been illustrated in Fig. S1. FTIR spectra of CS and *Mnos*-CS (Fig. S2), which demonstrate the successful synthesis of *Mnos*-CS. The *Mnos*-CS shows IR peaks at 1383 and 1645 cm^{-1} corresponding to N-C group stretching in introduced thioketone group (from CS where N-C group stretching of ketone group at 1377 cm^{-1}), -CO stretching in introduced thioamide group (from CS where amide -CO stretching at 1633 cm^{-1}), respectively. While other bands 1071 and 2980 and cm^{-1} slightly shifts from original bands of CS. These results confirmed the synthesis of *Mnos*-CS product.

Nanocapsules Fabrication and Characterization

Nanocapsules were fabricated through deposition of cationic polymer on the oil/water interface of nanoemulsion intermediate (Fig. 1). To optimize polymer concentration for nanocapsule formulations, the change in zeta potential was measured and optimum amount was obtained when no significant change in zeta potential was observed after increasing the polymer concentration. With increasing polymer proportion, the zeta potential rapidly increased to positive values. The zeta potentials of nanocapsules at various concentrations of polymers are shown in Fig. 2a. The optimum CS and *Mnos*-CS polymer concentration was found to be 0.6% *w*/*v* and 1.2% *w*/*v*, respectively for CNc-AB and *Mnos*CNc-AB nanocapsules (Fig. 2a). Particle characteristics of optimized nanocapsule formulations in terms of size (PDI) and zeta potential were 160.7 ± 7.53 nm (0.129 ± 0.03) and +28.2 ± 1.28 mV for CNc-AB, and 197.8 ± 8.84 nm (0.115 ± 0.04) and +31.7 ± 1.03 mV for *Mnos*CNc-AB, while for nanoemulsion intermediate were 116.8 ± 8.03 nm (0.102 ± 0.04) and −22.7 ± 1.54 mV. The sizes of nanocapsule formulations (CNc-AB and *Mnos*CNc-AB) were larger than that of the nanoemulsion intermediate. This increase in particle size was a first indication of the deposition of CS or *Mnos*-CS at the oil/water interface of nanoemulsion. Polymer incorporation at oil/water interface of nanoemulsion droplets results in change of zeta potential from negative to positive and this diversity in superficial charge of the carrier system is the second evidence of the polymer deposition. Developed nanocapsules were well dispersed without aggregation, showing near perfect Gaussian size distribution (Fig. 2b). Developed nanocapsules were found to be highly efficient for AB encapsulation with 97.5 ± 1.13% EE and 10.14 ± 0.07% DL for *Mnos*CNc-AB, while 96.2 ± 1.08% EE and 9.02 ± 0.09% DL in case of CNc-AB. Figure 2c shows the cumulative percentages of AB released in time-dependent manner from nanocapsules. The initial fast release can be ascribed to the cargo near the nanocapsule surface, while the slower and sustained release may be from the diffusion of the cargo inside the nanocapsule or be facilitated by the water-mediated erosion of the polymer matrix. The release of AB increased after mannosylation of nanocapsules. The results of the *in vitro* stability studies showed non-significant changes in particle size or encapsulated drug content indicating good stability in used media, as indicated in Fig. 2d.

Evaluation of Targeting Effect of Nanocapsules

Macrophage Uptake of Fluorescent Nanocapsules

The percentage of macrophage uptake can be related to percentage of cells allied with FITC fluorescence. Figure 3 shows the macrophage uptake efficiencies of nanocapsule by J774A.1 after 6 h incubation at 37°C. This study represents comparative uptake among CNc and *Mnos*CNc. The uptake percentage of *Mnos*CNc-FAB was 4.18 fold higher than that for CNc-FAB by infected macrophages, whereas, 1.49 fold higher *Mnos*CNc-FAB uptake capacity than that for CNc-FAB by non-infected macrophages.

Ex Vivo Imaging of Tissue Localized Nanocapsules

In vivo tissue localization of *Mnos*CNc-FAB, CNc-FAB and FAB was assessed through *ex vivo imaging* by observation of intensity of fluorescence using fluorescence photomicrographs of the harvested spleen, liver, lung, kidney and heart samples (Fig. 4). The fluorescence observed in *Mnos*CNc-FAB treated mice group was relatively higher than CNc-FAB and FAB in the liver and spleen sections while fluorescence intensity was highest in kidney section of FAB treated mice group.

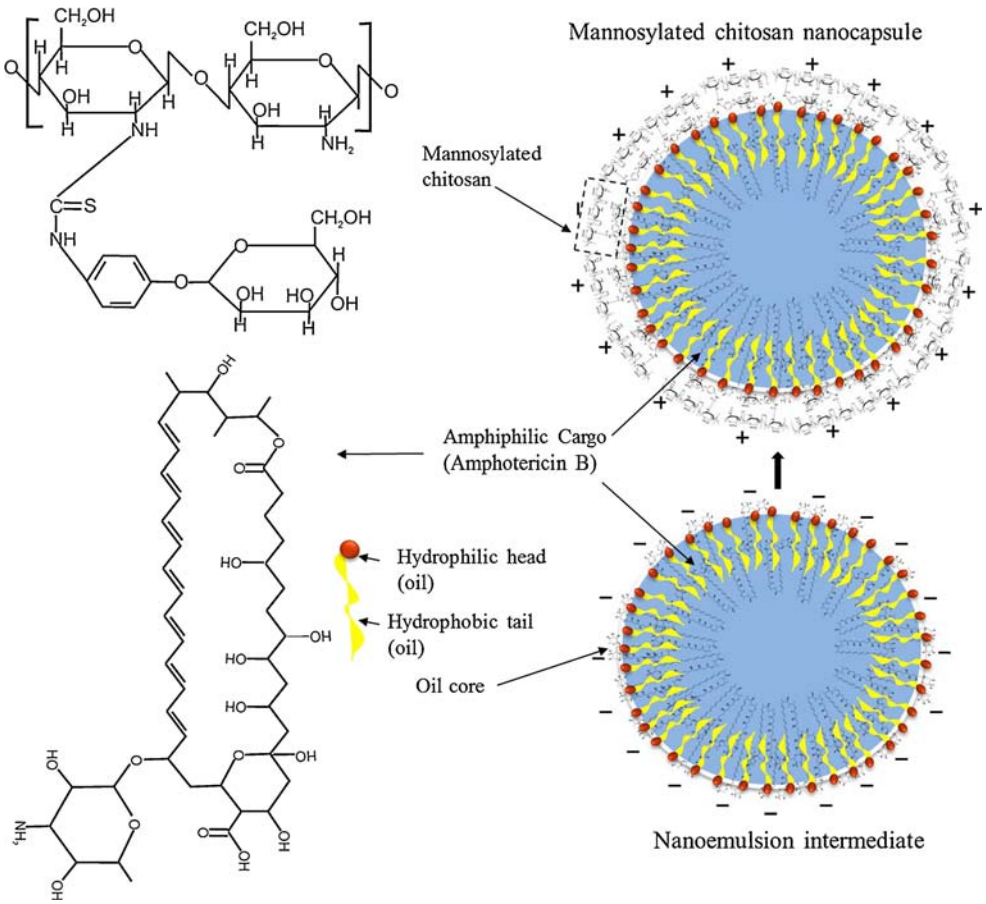

Fig. 1 Schematic presentation of mannosylated chitosan nanocapsule generation through deposition of mannosylated chitosan on oil/water interface of nanoemulsion intermediate.

In Vivo Distribution of AB-nanocapsules in Rats

The blood concentration-time profiles and pharmacokinetic parameters after the intravenous administration of AB via different carrier forms in rats at a dose of 1 mg/kg are presented in Fig. 5 and Table I, respectively. AB formulated in *Mnos*CNc showed lower plasma cargo concentration and higher tissue concentration compared to CNc-AB and AB, due to rapid clearance from blood correlated well with MMR mediated quick recognization and endocytosis within macrophage rich organs (i.e. liver, spleen etc.), as shown in Fig. 5. Higher rate of clearance and higher MRT was observed in *Mnos*CNc-AB compared with CNc-AB and AB. Blood clearance of *Mnos*CNc delivered cargo was 1.2-fold and 1.6-fold higher than that for CNc-AB and free AB. The data showed non-linear saturation like kinetic profile of *Mnos*-CNc-AB resulting in sustained plasma levels and increased mean residence time (MRT) within body. The MRT calculated for *Mnos*CNc-AB was 37.17±8.52 h, about 1.2-fold higher than that of CNc-AB and 2.3-fold higher than that of free AB. The AUC of *Mnos*CNc-AB will be significantly minimized based on the plasma profile as shown in Fig. 5. The *Mnos*CNc-AB showed prime cargo distribution in the spleen and liver, followed by the lung, kidney, to a lesser extent, in heart at all time points compared with CNc-AB and AB ($p<0.05$).

Assessment of Antileishmanial Activity and Immune-Alteration Profile

In Vitro Against Intra-macrophage Amastigotes

In vitro activity was tested against intracellular amastigotes incubated in culture medium, results are presented in Fig. 6a and b. The IC_{50} values demonstrated that *Mnos*CNc-AB has 1.69 and 2.46 times higher antileishmanial potential than that of CNc-AB and AB, respectively after 48 h. Furthermore cargo free *Mnos*CNc also illustrated remarkable parasite growth inhibition as shown in Fig. 6a.

In Vivo Against L. donovani Infected Hamsters

The results of an *in vivo* experiment (Fig. 6c) clearly manifested significant parasite growth inhibition (90.8±8.63% inhibition) in *Mnos*CNc-AB treated group than CNc-AB (85.2±6.21% inhibition), whereas 53.3±5.27% parasite inhibition was

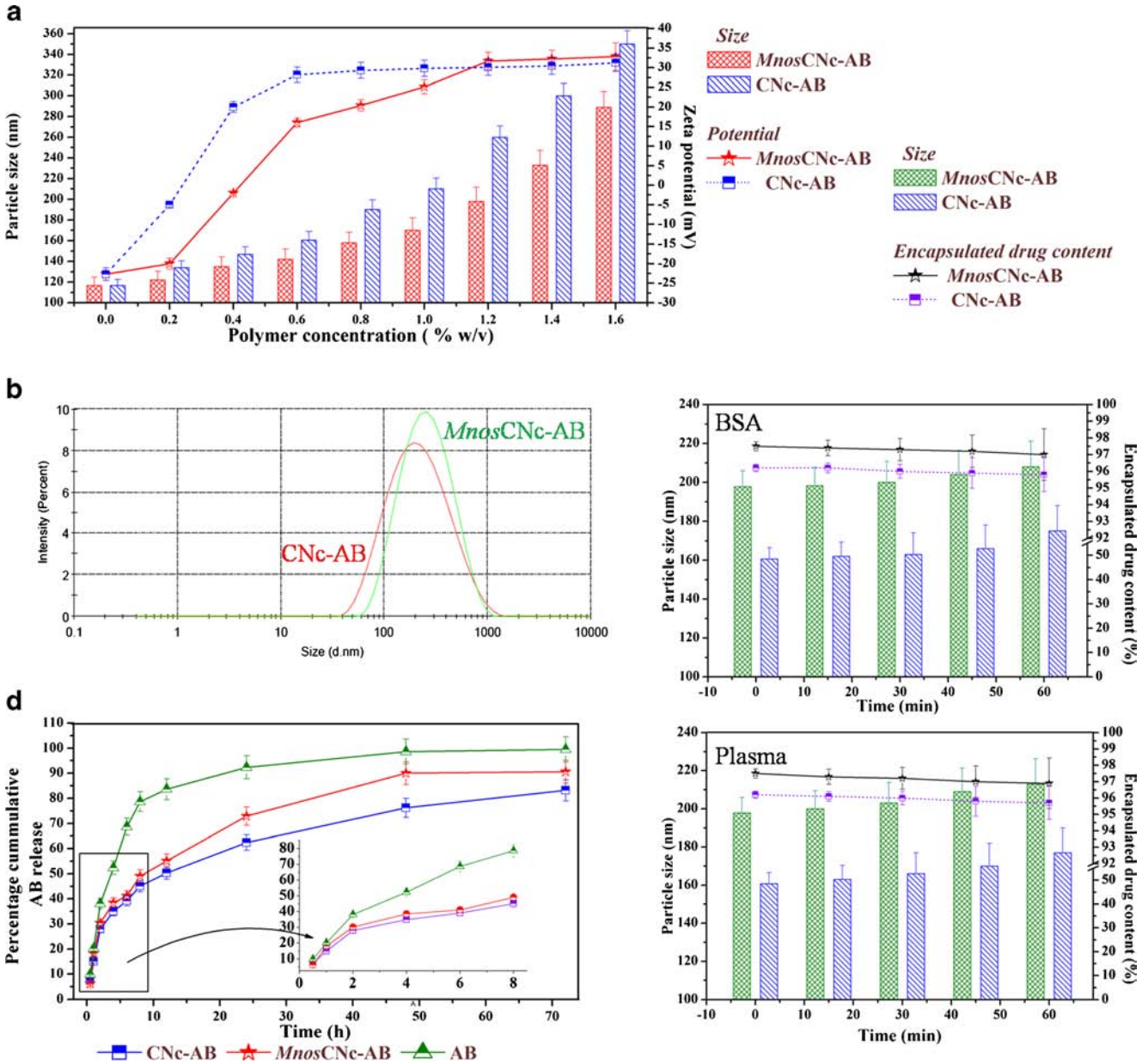

Fig. 2 (**a**) Zeta potential values of nanocapsule formulations at different concentrations (0–1.6%*w/v*) of polymer (CS or *Mnos*-CS) deposited at the oil/water interface of nanoemulsion intermediate after 24 h at 25°C. Values are expressed as mean ± SD ($n = 3$), (**b**) Particle size distribution of nanocapsules, measured using Photon Correlation Spectroscopy, showing formulation near perfect Gaussian size distribution, (**c**) *In vitro* cargo release profile of CNc-AB and *Mnos*CNc-AB using dialysis membrane diffusion technique with 0.5%*v/v* Tween 80 in PBS, pH 7.4 at different time intervals. Values are expressed as mean ± SD ($n = 3$), (**d**) Stability study of nanocapsules after incubation with 10% BSA and 10% plasma, at room temperature. At different time points, an aliquot of test suspension was removed to measure nanocapsule size and encapsulated drug (cargo) content, and results are expressed as mean ± SD ($n = 3$).

observed with free AB. Further, cargo free *Mnos*CNc itself able to result in 25.2 ± 2.42% parasite growth inhibition.

In Vivo Immune-Alteration Profile Against L. donovani Infected Hamsters. In order to evaluate the immune-alterations, cytokine and iNOS production was assessed in splenocytes of differently treated infected hamsters by qRT-PCR at 30 days post-infection. *Mnos*CNc-AB treated hamster group showed Th-1 dominance, evident from 3.2-fold higher IFN-γ level. In contrast, AB treated group expressed negligible IFN-γ enhancement. Elevated IFN-γ in *Mnos*CNc-AB treated group correlated with simultaneous upregulation of IL-12 (3.0-fold) and TNF-α (2.7-fold) cytokine expression (Fig. 7). Moreover, *Mnos*CNc-AB treated group showed suppress levels of IL-4, IL-10 and TGF-β immunosuppressive cytokines. Th-1 dominance in *Mnos*CNc-AB treated hamsters also correlated with 2.5-fold higher iNOS production than infected control. Cargo free *Mnos*CNc, at equivalent formulation amount, induced

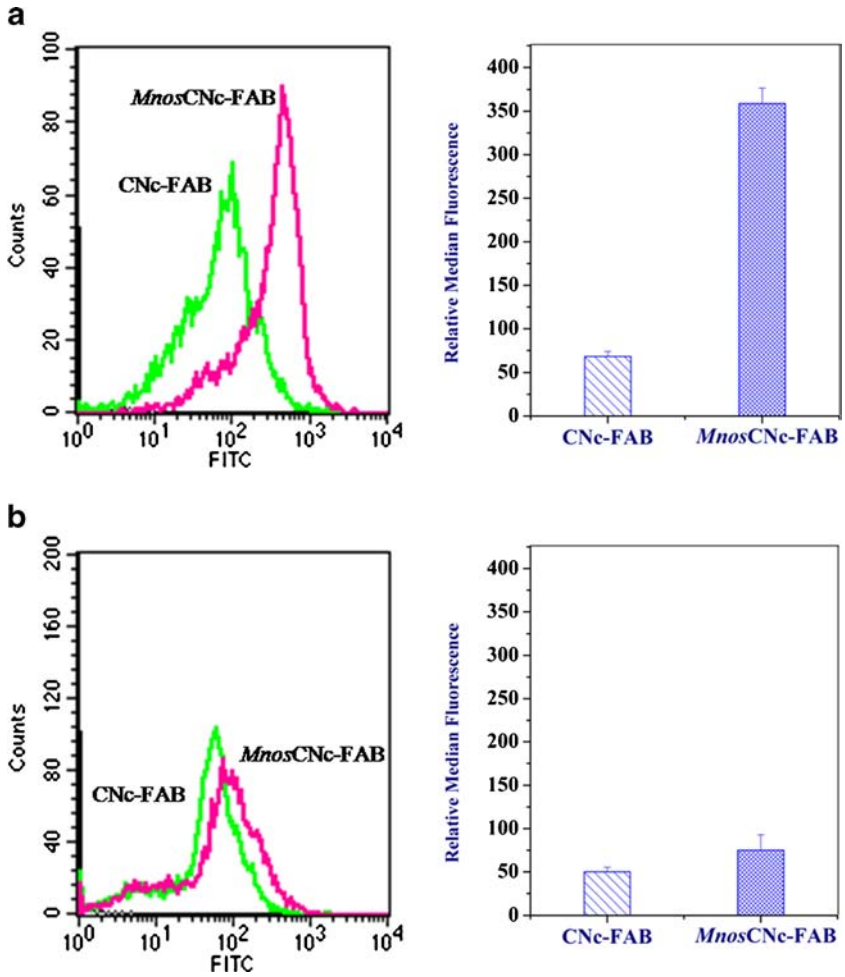

Fig. 3 *In vitro* uptake efficiency in macrophage J774A.1 cells after 6 h incubation with FITC tagged CNc-FAB and *Mnos*CNc-FAB. Values are expressed as mean ± SD ($n = 3$).

significantly elevated levels of tested Th-1 cytokines and iNOS, and suppressed levels of Th-2 cytokines. However, slight changes in cytokine levels were noted in supernatants from spleen aspirates of AB treated hamsters.

Toxicity Assessment

In Vitro Toxicity Assay

AB-Nanocapsules Hemo-compatibility. Incubation of erythrocytes with AB-nanocapsules at the concentration range of 0.5–25 µg/ml exhibited non-significant hemoglobin release compared to erythrocytes incubated with free AB (Fig. 8a). Analysis of data revealed that un-encapsulated free AB cargo often resulted in hemotoxicity upto 100%, while encapsulated cargo within *Mnos*CNc-AB and CNc-AB exhibited reduced hemotoxicity upto 2.38 ± 0.31% and 4.21 ± 0.52%, respectively at 25 µg/ml (Fig. 8a).

Effect of AB-nanocapsules on Macrophage Cell Viability. The cytotoxicity induced by AB-nanocapsules at the concentration range of 0.5–2.5 µg/ml is shown in Fig. 8b. The rank order of cytotoxicity against the J774A.1 macrophage cell line was *Mnos*CNc-AB<CNc-AB<AB. Results demonstrated negligible cytotoxicity of manosylated AB-nanocapsules, *in vitro*. Moreover, during the 48 h period *in vivo*, the experimental animals did not indicate any visible symptoms of toxicity associated to the injection of nanocapsules, while free AB cargo showed the toxicity symptoms.

In Vivo Toxicity Assay

Subacute Toxicity. The biochemical analysis in mice revealed that plain AB showed marked increase in the hepatotoxicity leading to the elevated levels of serum aspartate aminotransferase (ASAT) and alanine aminotransferase (ALAT). In contrast, administration of CNc-AB and *Mnos*CNc-AB, did not show any significant increase in the serum ASAT and ALAT levels. The plain AB treated mice group had significant increase (>3 fold) ($p < 0.05$) in serum creatinine and BUN level over control, indicating nephrotoxicity (Fig. 8c).

Single Dose Acute Toxicity Studies. Acute toxicity results suggest that only 20% mortality was found in mice at the dose upto

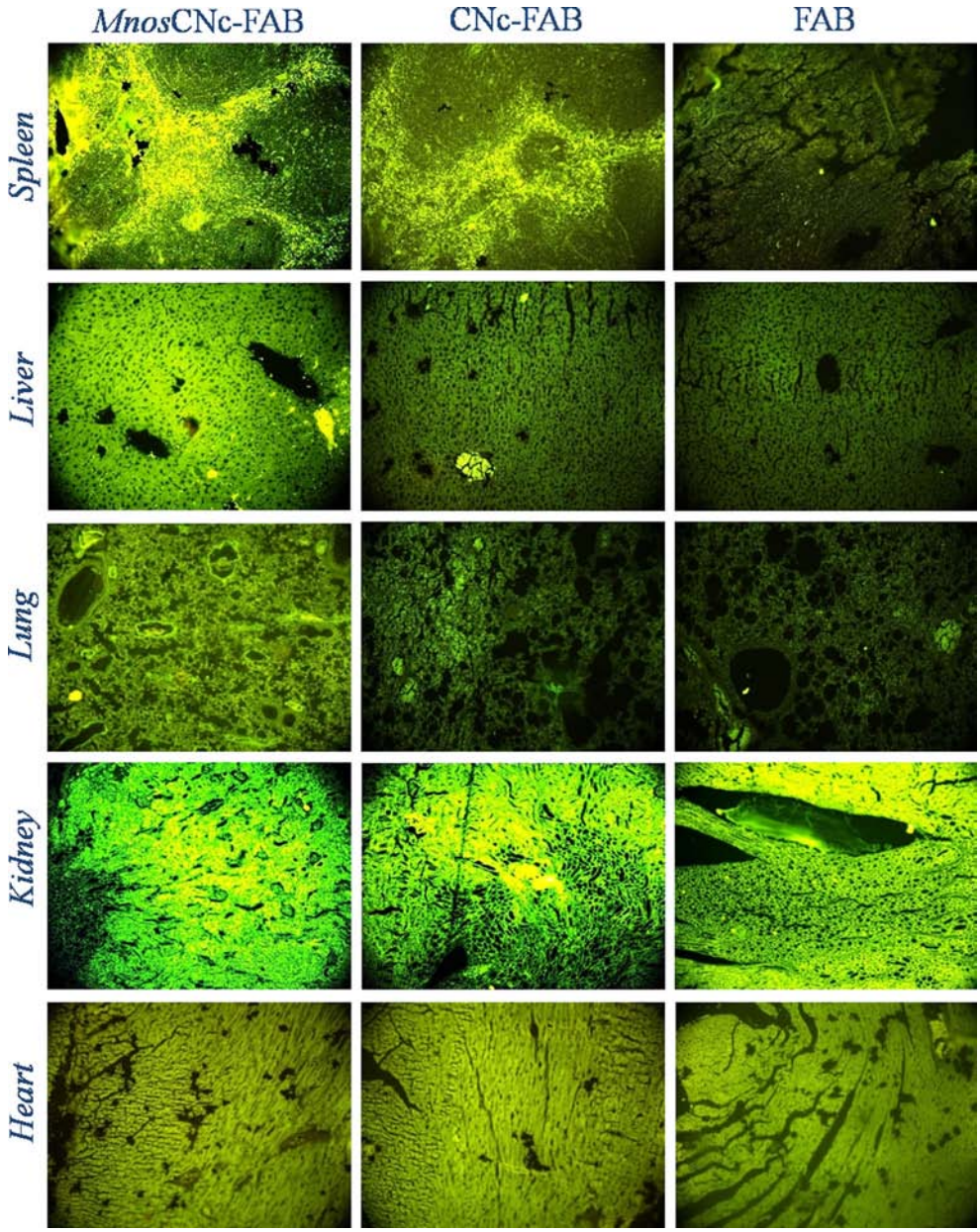

Fig. 4 *In vivo* tissue localization of FITC tagged FAB, CNc-FAB and *Mnos*CNc-FAB in liver, Spleen, lung, kidney and heart following intravenous administration of AB equivalent 1 mg/kg for consecutive three days. The tissues were harvested after 2 h of last administration.

20 mg/kg for *Mnos*CNc-AB while 40% mortality was observed with CNc-AB at same dose as showed in Fig. 8d. Mice injected with *Mnos*CNc-AB and CNc-AB showed more tolerance to the cargo as revealed by the high tolerated dose (20 mg/kg) of encapsulated AB as compared to free AB, while 100% mortality was observed in mice treated with AB only at 5 mg/kg dose as showed in Fig. 8d, which prevented us to increase the dose further.

DISCUSSION

An important step in the advancement of Amphotericin B mediated chemotherapy is the development of an efficient, macrophage targeted cargo delivery system to facilitate the desired action and eliminate undesired side action. It is well accepted that, successful *in vivo* cargo delivery for intravenous administration for dreaded disease like leishmaniasis may require not just a well-defined nanostructure but also target specific-delivery potential. Receptor-mediated endocytosis is a promising cargo delivery technique. Infected macrophages have enormous expression of mannose receptors on their surface, may provide directive route for facilitated receptor-mediated endocytosis to cargo encapsulated carriers possessing MMR receptor-specific ligand.

In a previous study, we have developed chitosan nanocapsules as an AB carrier (CNc-AB) (8). CNc-AB showed

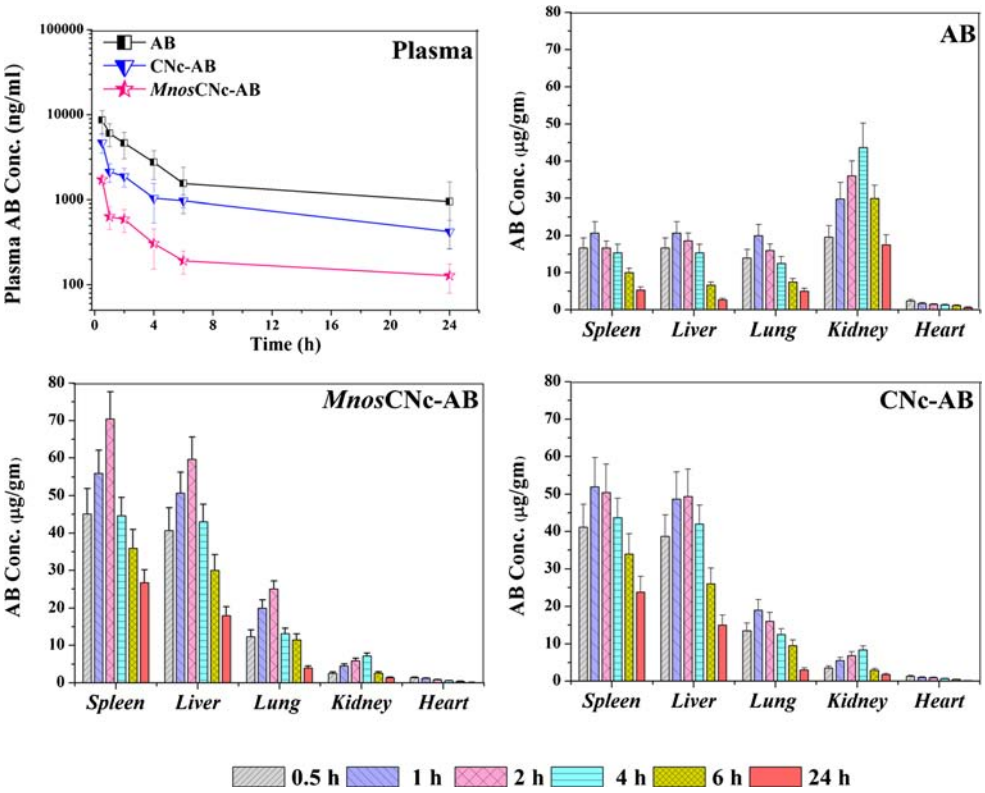

Fig. 5 Biodistribution profiles of AB at various time points in plasma, spleen, liver, kidney, heart and lung of wistar rats after i.v. administration of plain AB, CNc-AB and *Mnos*CNc-AB at 1 mg/kg dose, Values are expressed as mean ± SD ($n = 3$).

good macrophage cell viability and hemo-compatibility but poor cell specificity. Consequently, to obtain both macrophage cell specificity and to reduce toxic manifestations, *Mnos*-CS copolymer was synthesized using mannopyranosylphenyl isothiocyanate and low molecular weight chitosan, formulated in nanocapsules and continued evaluation studies in order to realize a rapid clearance from systemic circulation and macrophage targeting potential.

Since literature suggested mannose as the most appropriate ligand for MMR (4), *Mnos*CNc formulation was evaluated for its targeting efficiency and *in vivo* distribution after intravenous injection to obtain a safe non-toxic formulation against leishmaniasis, while CNc-AB and plain AB were included for comparison.

Table I Pharmacokinetic Parameters of AB After Intravenous Administration of AB-encapsulated Formulations in Rats at a Dose of 1 mg AB/kg (Mean ± SD, $n = 3$)

AB equivalent concentration in formulation	$t_{1/2}$ (h)	AUC_{0-24} ($\mu g\ h\ ml^{-1}$)	MRT (h)	CL ($ml\ h^{-1}\ kg^{-1}$)
CNc-AB	30.32 ± 6.53	34.08 ± 7.53	30.09 ± 6.43	66.53 ± 5.28
*Mnos*CNc-AB	37.03 ± 9.61	26.23 ± 6.51	37.17 ± 8.52	80.28 ± 6.97
Plain AB	18.15 ± 3.42	38.16 ± 3.42	16.28 ± 2.05	49.12 ± 7.74

Abbreviations: $t_{1/2}$ half life, AUC_{0-24} Area under the cargo concentration-time curve from 0 to 24 h, MRT_{0-24} mean residence time, *CL* clearance; the pharmacokinetic parameters were calculated by our own experiments

In our study, we constructed nanocapsules through 'insertion' of the *Mnos*-CS/CS polymer in the outer surface layer of the nanoemulsion droplets induced by solvent evaporation and probably due to electrostatic interactions between the amino groups of polycationic *Mnos*-CS/CS and, the carboxyl and phosphate groups of negatively charged emulsion components. The 0.6% and 1.2%*w/v* concentration of CS or *Mnos*-CS was found to be optimum because there was no further change in zeta potential when concentration was further increased (Fig. 2a). The zeta potential is an important characteristic of delivery system as it can influence stability as well as cell adhesion. Positive potential of delivery system play prominent role in its binding to anionic cell surfaces, which facilitates cellular uptake (17), and herein, positivity of final nanocapsules is accountable for adsorption mediated endocytosis. On the other hand, cationic polymeric layers around nanoemulsion droplets able to provide long term stability to delivery system in biological fluids (serum, plasma) by preventing adsorption of cationic proteins and ions which have tendency to breakdown the negatively charged system, thereby leakage of the entrapped agents (8). The adsorption of *Mnos*-CS or CS over the nanoemulsion droplet was confirmed by reversal of the zeta potential. Furthermore, entrapment of amphiphilic AB cargo molecule between hydrophilic polymer and hydrophobic cavitation nanoemulsion core (18), results in higher entrapment efficiency. The *in vitro* release results suggest that moderate modification of CS did not evidently influence the *in vitro* release behavior of CNc nanocapsules.

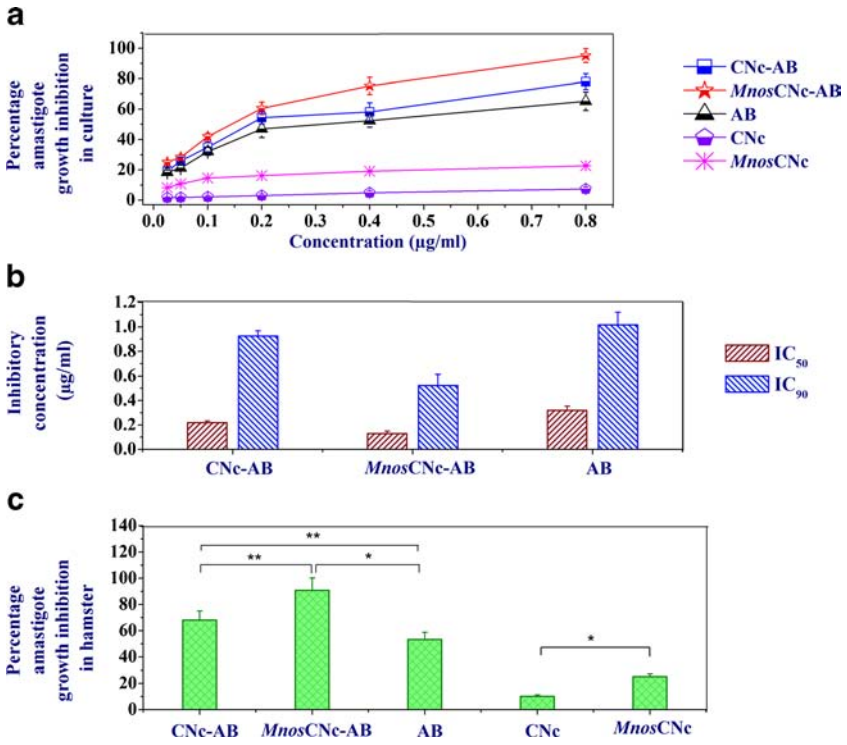

Fig. 6 Assessment of antileishmanial activity where all values are expressed as mean ± SD (**a**) *In vitro* dose–response curve ($n = 5$), (**b**) *In vitro* activity (IC_{50} and IC_{90}) against *L. donovani* amastigote infected macrophages after 48 h incubation ($n = 5$), (**c**) *In vivo* activity against established infection of *L. donovani* in hamsters. Cargo formulations and plain AB (equivalent to 1 mg/kg/day for 5 consecutive days) and formulations without cargo were injected intraperitoneally into infected Syrian golden hamsters ($n = 5$). (*$P < 0.05$, **$P < 0.01$).

However, moderate acceleration of AB release from *Mnos*CNc may be attributed to comparatively more hydrophilic behavior of mannose moieties. In case of nanocapsule, positive polymer-surfactant layers around nanoemulsion droplets provided long term stability, attributed to strong repulsion to cationic proteins and, cations (Na^+, Ca^{++}) that are present in the biological fluids thereby preventing aggregation.

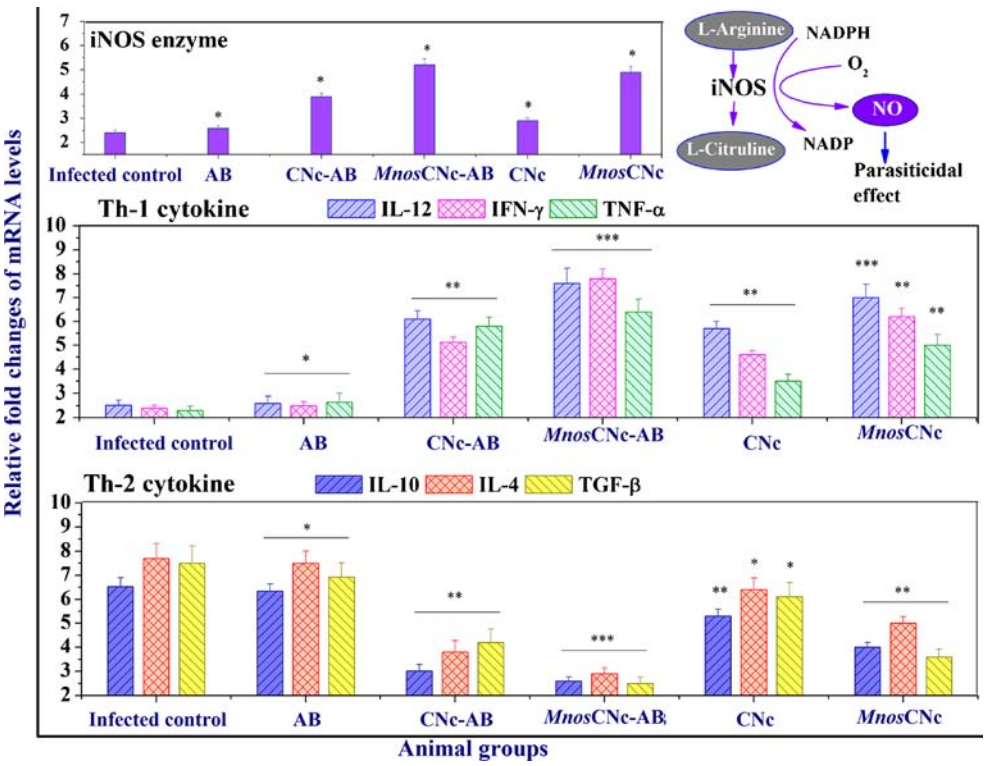

Fig. 7 *In vivo* immuno-modulatory responses concerning splenic cytokines (IL-12, IFN-γ, TNF-α, IL-12, IL-4, IL-10 and TGF-β) and enzyme iNOS mRNA expression in infected control and treated hamsters by quantitative RT-PCR. Analysis showing the relative fold changes of iNOS and cytokine expression level ± SD. ($n = 5$ hamsters/time point) in comparison to reference gene (HPRT). The significant values indicate differences between fold changes of treated groups with infected control groups. (*$p < 0.05$, **$p < 0.01$, ***$p < 0.001$).

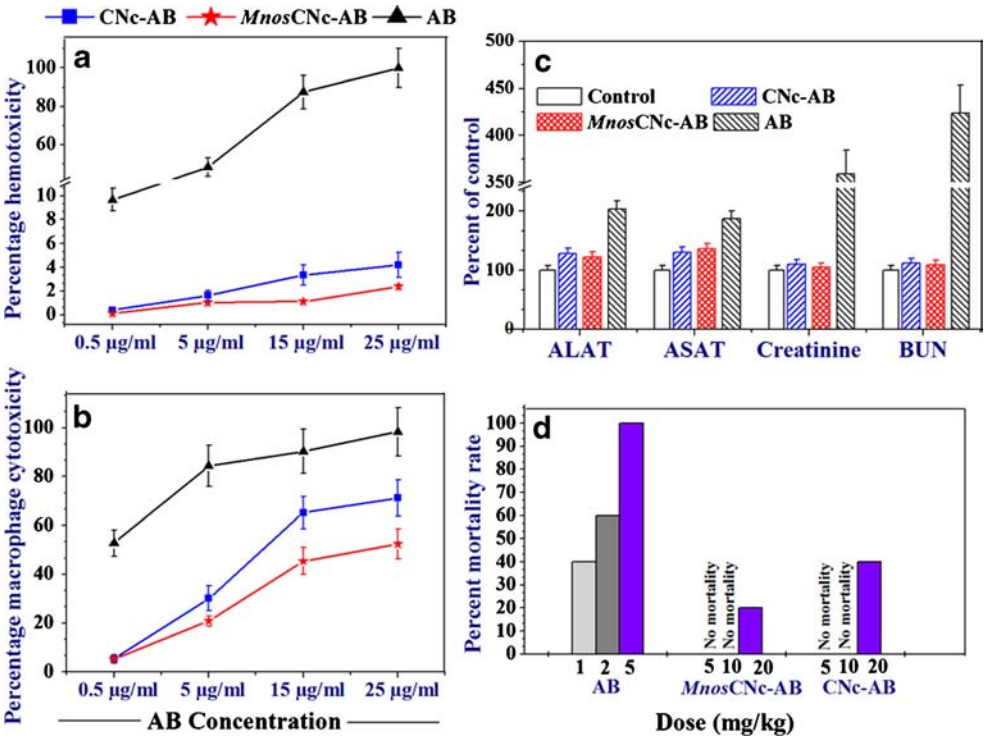

Fig. 8 AB toxicity study against (**a**) erythrocytes after 2 h incubation ($n = 5$), (**b**) J774A.1 macrophage cells after 48 h incubation ($n = 5$), (**c**) mice groups at the intravenous dose of 1 mg/kg daily for 14 days ($n = 3$) while one additional mice group as control received saline. Subacute toxicity was measured by serum biochemical analysis of transaminases: ASAT and ALAT, creatinine and BUN elicited from experimental mice, (**d**) twelve mice groups ($n = 6$) received intraperitoneal dose of 5, 10 and 20 mg/kg each for CNc-AB and *Mnos*CNc-AB while 1, 2, 5 mg/kg for plain AB. Acute toxicity was evaluated in terms of percent mortality rate. All toxicity data are expressed as mean ± SD.

An ideal characteristic of targeted cargo delivery system is blood circulatory half-life that determines the targeting capability of the formulation and availability of the drug that can reach the target cells. Meanwhile, uptake of delivery system by MPS macrophages is responsible for the major loss of system from systemic circulation. To evaluate target delivery effects, prior to *in vivo* experiment, *in vitro* macrophage uptake assay was conducted to predict the phagocytosis of nanocapsules by macrophages. The evidence presented in macrophage uptake studies demonstrate 4.18 fold greater uptake of *Mnos*CNc-FAB over CNc-FAB by infected macrophages, overexpressing MMR specific for mannose ligand (4,19), following receptor mediated active targeting approach (4). While non-infected macrophages have 1.49 fold superior *Mnos*CNc-FAB uptake capacity than that for CNc-FAB, following size and adsorption mediated passive targeting approach (Fig. 3). This higher uptake of *Mnos*CNc-FAB compared with CNc-FAB in macrophages is of interest in the sense that there is tendency for the enhanced localization of and enhanced distribution of encapsulated cargo (through *Mnos*CNc-AB) by, mannose modified nanocapsules in macrophage enriched organs (liver and spleen) as observed from tissue localization (Fig. 4) and organ distribution studies (Fig. 5).

Pharmacokinetic parameters demonstrated lower AB level in plasma delivered by mannosylated nanocapsules (*Mnos*CNc-AB) and high clearance rate compared to CNc-AB and free AB (Fig. 5 and Table I). Data indicate that *Mnos*CNc-AB was quickly recognized by MPS from the systemic circulation while CNc-AB and AB exhibited a markedly delayed recognization (Fig. 5). Comparative evaluation of *in vitro* macrophage uptake data and, *in vivo* tissue localization and blood clearance data clearly revealed that, higher the phagocytosis *in vitro*, higher the localization in macrophage rich tissues (liver and spleen) and shorter the systemic circulation *in vivo*. Comparatively higher cargo amount delivered by mannosylated nanocapsules than by CNc and plain AB in both liver and spleen demonstrate that most of the cargo is rapidly localized in these organs due to enhanced uptake by macrophages, which may be significant for visceral leishmaniasis. The significant increased uptake of *Mnos*CNc was probably due to the 'identifiable' surface created by *Mnos*-CS layering, which effectively supervise the recognition and enhanced uptake by MPS macrophages and thus increase the MPS organ deposition. The enhanced uptake of *Mnos*CNc compared to CNc is possibly due to the fact that primary determinant of mannose specificity in CRD on mannose receptor is the presence of hydroxyl groups in positions equivalent to equatorial 3 and 4- hydroxyl groups of D-mannose. In addition, minute localization and less distribution of AB in macrophage deficient organs (heart, kidney and lung) delivered by *Mnos*CNc-AB (Fig. 5) is responsible for reduction in AB related toxic manifestations. While plain AB was distributed evenly between liver, spleen and lung but higher disposition towards kidney (20), as illustrated in Fig. 5 is accountable for AB mediated nephrotoxicity.

The desired tissue localization, enhanced macrophage uptake and biodistribution profile of mannosylated nanocapsules is responsible for significantly improved antileishmanial

activity of *Mnos*CNc-AB when compared with CNc-AB ($P<0.05$) in eliminating intracellular amastigotes of *L. donovani* in both an *in vitro* macrophage model and an *in vivo* hamster model of VL (Fig. 6). Our data showed that *Mnos*CNc could be a useful carrier for targeting antileishmanial cargos into macrophage.

Nevertheless, mannosylated nanocapsules produce a signal for engulfment by phagocytes, get specifically recognized and phagocytosed by macrophages, which subsequently leads to macrophage activation and secretion of pro-inflammatory cytokines. Macrophage activation leads to rapid parasite killing and digestion (21). Herein, we analyzed Th-1 and Th-2 cytokines (IFN-γ, TNF-α, IL-12, TGF-β, IL-4 and IL-10) and iNOS enzyme to investigate their contribution in treatment of *Leishmania* infected hamsters through administration of cargo free and cargo loaded nanocapsules. The results of present study demonstrated that mannose modified nanocapsules induce significantly elevated release of the IL-12, IFN-γ and TNF-α cytokines (Fig. 7) through macrophage activation. Elevation of iNOS enzyme results in increase in nitric oxide (NO) production through conversion of L-arginine to L-citruline. NO has efficient parasiticidal activity and plays important role to treat infected macrophages during experimental infection (22,23). The *Mnos*CNc has been shown to induce the iNOS pathway, which results in subsequent production of NO (24). Concurrently, result exhibited favorable reduction of infection susceptible IL-10, IL-4 and TGF-β gene expression, which are potent inhibitors of macrophage activation and killing of *Leishmania* organisms. These regulatory effects of *Mnos*CNc on pro-inflammatory cytokines clearly confirmed the potential of the targeted nanocapsules for splenic macrophages and ensured Th-1 mediated protection. The powerful ability to suppress disease promoting IL-10, IL-4 and TGF-β and to effectively trigger macrophage microbicidal NO molecule promoting iNOS thus reversing the immunosuppressive condition towards Th-1 type immune response, accounts for prominent cure provided by *Mnos*CNc-AB.

To evaluate the safety profile, a cell viability study was carried out in non-infected J774A.1 macrophage cells. In the current study, the cell viability was further increased using mannosylated chitosan nanocapsules which is attributed to the alkane (CH_2-CH_2) bridge between mannose and chitosan. The cell viability produced by *Mnos*CNc-AB (47.6% of control) was higher than that of CNc-AB (29.3% of control) at a concentration of 25 μg/ml in the J774A.1 cells. Hematological intolerance of AB encapsulated within nanocapsules was also evaluated. In this aspect AB-induced hemolysis was studied *in vitro* which is a reliable measure for estimating the membrane damage caused *in vivo*. Almost negligible hemolytic activity of AB encapsulated in nanocapsules compared to free AB, demonstrated no deleterious effects on erythrocytes owing to the dominated monomeric molecular state of encapsulated cargo molecule within nanocapsules. Whereas, toxic manisfestations of unencapsulated free AB correlated to its molecular organization within dimeric and multimeric aggregation states, as analyzed by UV-visible spectroscopy (Data provided in supplementary sheet). Study observation complies with the published report wherein high toxicity of AB to human erythrocytes and other cultured mammalian cells correlated with the aggregated form compared to the non-toxic monomeric form of the drug (14).

Nephrotoxicity is the major undesired side effect of AB responsible for its limited clinical applications and is usually manifested by renal insufficiency due to the abnormalities in glomerulus and tubular function. In general, AB-induced nephrotoxicity is characterized by increased serum creatinine and blood urea levels as biochemical markers, which are routinely evaluated as an indicator of clinical renal function. Muscle metabolism end product creatinine that gets filtered and excreted by kidney is important indicative of renal dysfunction, was found to be significantly lower in *Mnos*CNc-AB treated mice compared to AB and CNc-AB mice groups. Similarly, abnormal increase in blood urea levels represents the dysfunction or damage to the kidney, and was found to be comparatively low in *Mnos*CNc-AB treated mice group (Fig. 8c). Significantly lower levels of serum creatinine and blood urea in the mice, indicating lower nephrotoxicity by *Mnos*CNc-AB compared to AB and CNc-AB. Additionally, the biochemical analysis revealed that AB illustrated marked increase in the hepatotoxicity leading to the elevated levels of serum ASAT and ALAT (Fig. 8c), complies with reported study (25). In contrast, administration of AB encapsulated nanocapsules in mice did not show any significant increase in the serum transaminase levels. Furthermore, the acute toxicity results (Fig. 8d) clearly demonstrated that AB formulated in *Mnos*CNc is safer than free AB as well as CNc-AB which might permit the administration of much higher doses of the cargo, leading to an increase on the efficacy of the pharmaceutical product in the leishmaniasis treatment.

CONCLUSIONS

The present investigation provides evidence that the prototype formulation may be used for efficient treatment of leishmaniasis via MMR-specific mannosylated nanocapsules bearing AB. *Mnos*CNc had undergone the notable desired macrophage uptake, that led to a dramatic shortening in their presence in systemic circulation while higher distribution of mannosylated nanocapsules to macrophage rich organs (spleen and liver). This resulted in activation of parasite infected macrophages and release of encapsulated cargo at desired intracellular site within macrophages to pronounce the parasiticidal effect and undesirable AB-mediated side effects were eliminated due to restricted distribution to renal tissues.

ACKNOWLEDGMENTS AND DISCLOSURES

Authors would like to acknowledge the financial assistance received from Department of Science and Technology, Government of India [SR/SO/HS-218/2012] and CSIR Network project HOPE. We thank Sophisticated Analytical Instrument Facility Division, CSIR-CDRI, Lucknow for flow cytometry analysis. This is CSIR-CDRI communication 8909.

Transparency Declaration Section None to declare.

REFERENCES

1. Dupont B. Overview of the lipid formulations of amphotericin B. J Antimicrob Chemother. 2002;49 Suppl 1:31–6.
2. Patel GP, Crank CW, Leikin JB. An evaluation of hepatotoxicity and nephrotoxicity of liposomal amphotericin B (L-AMB). J Med Toxicol. 2011;7:12–5.
3. Asthana S, Gupta PK, Chaurasia M, Dube A, Chourasia MK. Polymeric colloidal particulate systems: intelligent tools for intracellular targeting of antileishmanial cargos. Expert Opin Drug Deliv. 2013;10:1633–51.
4. Stahland P, Gordon S. Expression of a mannosyl-fucosyl receptor for endocytosis on cultured primary macrophages and their hybrids. J Cell Biol. 1982;93:49–56.
5. Asthana S, Jaiswal AK, Gupta PK, Dube A, Chourasia MK. Th-1 biased immunomodulation and synergistic antileishmanial activity of stable cationic lipid-polymer hybrid nanoparticle: biodistribution and toxicity assessment of encapsulated amphotericin B. Eur J Pharm Biopharm Off J Arbeitsgemeinschaft Pharmazeutische Verfahrenstechnik eV. 2014.
6. Ezekowitz RA, Sastry K, Bailly P, Warner A. Molecular characterization of the human macrophage mannose receptor: demonstration of multiple carbohydrate recognition-like domains and phagocytosis of yeasts in Cos-1 cells. J Exp Med. 1990;172:1785–94.
7. Taylorand ME, Drickamer K. Structural requirements for high affinity binding of complex ligands by the macrophage mannose receptor. J Biol Chem. 1993;268:399–404.
8. Asthana S, Jaiswal AK, Gupta PK, Pawar VK, Dube A, Chourasia MK. Immunoadjuvant chemotherapy of visceral leishmaniasis in hamsters using amphotericin B-encapsulated nanoemulsion template-based chitosan nanocapsules. Antimicrob Agents Chemother. 2013;57:1714–22.
9. Mansouri S, Cuie Y, Winnik F, Shi Q, Lavigne P, Benderdour M, *et al.* Characterization of folate-chitosan-DNA nanoparticles for gene therapy. Biomaterials. 2006;27:2060–5.
10. Kim TH, Jin H, Kim HW, Cho MH, Cho CS. Mannosylated chitosan nanoparticle-based cytokine gene therapy suppressed cancer growth in BALB/c mice bearing CT-26 carcinoma cells. Mol Cancer Ther. 2006;5:1723–32.
11. Paiphansiri U, Tangboriboonrat P, Landfester K. Polymeric nanocapsules containing an antiseptic agent obtained by controlled nanoprecipitation onto water-in-oil miniemulsion droplets. Macromol Biosci. 2006;6:33–40.
12. Martini E, Fattal E, de Oliveira MC, Teixeira H. Effect of cationic lipid composition on properties of oligonucleotide/emulsion complexes: Physico-chemical and release studies. Int J Pharm. 2008;352:280–6.
13. Gupta PK, Jaiswal AK, Asthana S, Verma A, Kumar V, Shukla P, *et al.* Self assembled ionically sodium alginate cross-linked amphotericin B encapsulated glycol chitosan stearate nanoparticles: applicability in better chemotherapy and non-toxic delivery in visceral leishmaniasis. Pharm Res. 2014.
14. Gupta PK, Asthana S, Jaiswal AK, Kumar V, Verma AK, Shukla P, *et al.* Exploitation of lectinized lipo-polymerosome encapsulated Amphotericin B to target macrophages for effective chemotherapy of visceral leishmaniasis. Bioconjug Chem. 2014;25:1091–102.
15. Melby PC, Tryon VV, Chandrasekar B, Freeman GL. Cloning of Syrian hamster (Mesocricetus auratus) cytokine cDNAs and analysis of cytokine mRNA expression in experimental visceral leishmaniasis. Infect Immun. 1998;66:2135–42.
16. Gupta A, Asthana S, Konwar R, Chourasia MK. An insight into potential of nanoparticles-assisted chemotherapy of cancer using gemcitabine and its fatty acid prodrug: a comparative study. J Biomed Nanotechnol. 2013;9:915–25.
17. Kunath K, von Harpe A, Fischer D, Petersen H, Bickel U, Voigt K, *et al.* Low-molecular-weight polyethylenimine as a non-viral vector for DNA delivery: comparison of physicochemical properties, transfection efficiency and in vivo distribution with high-molecular-weight polyethylenimine. J Control Release. 2003;89:113–25.
18. Anton N, Benoit JP, Saulnier P. Design and production of nanoparticles formulated from nano-emulsion templates-a review. J Control Release. 2008;128:185–99.
19. Zhu L, Chen L, Cao QR, Chen D, Cui J. Preparation and evaluation of mannose receptor mediated macrophage targeting delivery system. J Control Release. 2011;152 Suppl 1:e190–1.
20. Andes D, Safdar N, Marchillo K, Conklin R. Pharmacokinetic-pharmacodynamic comparison of amphotericin B (AMB) and two lipid-associated AMB preparations, liposomal AMB and AMB lipid complex, in murine candidiasis models. Antimicrob Agents Chemother. 2006;50:674–84.
21. Nacy CA, Meltzer MS, Fortier AH. Macrophage activation to kill Leishmania tropica: characterization of P/J mouse macrophage defects for lymphokine-induced antimicrobial activities against Leishmania tropica amastigotes. J Immunol. 1984;133:3344–50.
22. Basu R, Bhaumik S, Basu JM, Naskar K, De T, Roy S. Kinetoplastid membrane protein-11 DNA vaccination induces complete protection against both pentavalent antimonial-sensitive and -resistant strains of Leishmania donovani that correlates with inducible nitric oxide synthase activity and IL-4 generation: evidence for mixed Th1- and Th2-like responses in visceral leishmaniasis. J Immunol. 2005;174:7160–71.
23. Zafra R, Jaber JR, Perez-Ecija RA, Barragan A, Martinez-Moreno A, Perez J. High iNOS expression in macrophages in canine leishmaniasis is associated with low intracellular parasite burden. Vet Immunol Immunopathol. 2008;123:353–9.
24. Sorimachi K, Akimoto K, Hattori Y, Ieiri T, Niwa A. Activation of macrophages by lactoferrin: secretion of TNF-alpha, IL-8 and NO. Biochem Mol Biol Int. 1997;43:79–87.
25. Larabi M, Pages N, Pons F, Appel M, Gulik A, Schlatter J, *et al.* Study of the toxicity of a new lipid complex formulation of amphotericin B. J Antimicrob Chemother. 2004;53:81–8.